

ARTICLES

Interpreting the Physical Background of Empirical Solvent Polarity via Photodetachment Spectroscopy of Microsolvated Aromatic Ketyl Anions

Toshihiko Maeyama,* Keiji Yoshida, Izumi Yagi, Asuka Fujii, and Naohiko Mikami

Department of Chemistry, Graduate School of Science, Tohoku University, Aoba-ku, Sendai 980-8578, Japan

Received: February 23, 2009; Revised Manuscript Received: June 24, 2009

The physical background of empirical solvent polarity is explored in regard to trends in solute–solvent intermolecular potential energy functions. Aromatic ketyl anions, benzophenone, and 9-fluorenone radical anions, are chosen for a model solute molecule showing solvatochromic behavior similar to betaine-30 dye, which provides the most established solvent polarity scale, $E_T(30)$. Common features among the ketyl anions and betaine-30 were examined with quantum chemical calculations for the electronic states and solvation structure. Vertical photodetachment and photoabsorption energies were determined for the ketyl anions microsolvated with a single solvent molecule by measuring photoelectron spectra as well as photodetachment excitation spectra for several aprotic and protic solvents. The spectroscopic data were analyzed through quantum chemical calculations based on density functional theory, and their relationship with the characteristics of intermolecular potential energies was considered. As a result, the typical solvent polarity parameter can be interpreted to reflect essentially the gradient of a potential energy function (namely, the strength of force) between a negative charge and the solvent molecules in the attractive region. A large polarity for protic solvents is attributed to an effective interaction of a proton-like hydrogen atom with the negative charge in a short-range.

1. Introduction

Solvent effect is one of the most fundamental research subjects in all fields of chemistry. It is common knowledge that solvation in a polar solvent considerably affects the physical and chemical performance of a solute molecule. Historically, great efforts have been made for unified understanding of solvation from an aspect of neat solvent's dielectric property. Many theoretical models for solvation have been proposed on the basis of the classical frameworks developed by Born¹ and Onsager,² assuming that a solute molecule resides in a spherical cavity of a certain radius in a continuum dielectric medium. However, these kinds of models^{3–5} are applicable only for aprotic solvents, and hardly for protic solvents having an OH or NH group. More quantitative treatments involving quantum chemical calculations^{6,7} or molecular dynamics simulations^{8,9} have recently advanced, although the physical picture of solvation is probably hidden by the complexity in a large number of molecules.

There is no simple way to predict the magnitude of solvent effects by using known physical constants for a neat solvent. An empirical parameter of “solvent polarity” is regarded to be a convenient index for a pragmatic purpose like building synthetic strategy. Numerous parameters^{10–12} were derived from experimentally observed constants for a solute molecule in different solvents, and mutual correlations among them were examined. The $E_T(30)$ scale¹⁰ proposed by Reichardt and Dimroth is the most widely used parameter of solvent polarity.

It corresponds to the energy of the first photoabsorption band peak of so-called betaine-30 dye (2,6-diphenyl-4-(2,4,6-triphenylpyridinio)phenoxide), which is a huge molecule containing seven aromatic rings and exhibits hypsochromic behavior (blue shifts) in polar solvents. Figure 1 shows plots of $E_T(30)$ values for several solvents¹¹ with respect to (a) dielectric constants and (b) molecular dipole moments.¹³ $E_T(30)$ values for aprotic solvents exhibit a crude correlation with dielectric constants as well as dipole moments. On the other hand, those for protic solvents are large, almost irrespective of the dielectric constants or dipole moments. Nevertheless, the applicability of the $E_T(30)$ scale has been established for a large number of both aprotic and protic solvents, because it shows a nicely linear correlation with solvent effects in various phenomena, e.g., the activation energy of solvolysis of *tert*-butylchloride determined with kinetic measurements.^{11,14} This fact leaves us one question, why the empirical rule in hierarchy of solvent polarity holds for solution systems of different solute molecules. It is plausible that the empirical polarity scale reflects a common tendency concerning to something about solute–solvent intermolecular interactions. However, it seems that neither experimental nor theoretical investigations have fully struggled with unraveling the physical source of the tendency. For example, in multiparameter fitting approaches^{15,16} for the solvent polarity, a solvent effect is factorized into contributions from hydrogen bonding and dipolar solvation in a phenomenological way without any evident theoretical basis, while the major part of both the interactions must originate from electrostatic terms.

Because solvatochromism of betaine-30 is frequently applied for the empirical polarity scale, modeling of its electronic

* To whom correspondence should be addressed. E-mail: tmaeyama@mail.tains.tohoku.ac.jp.

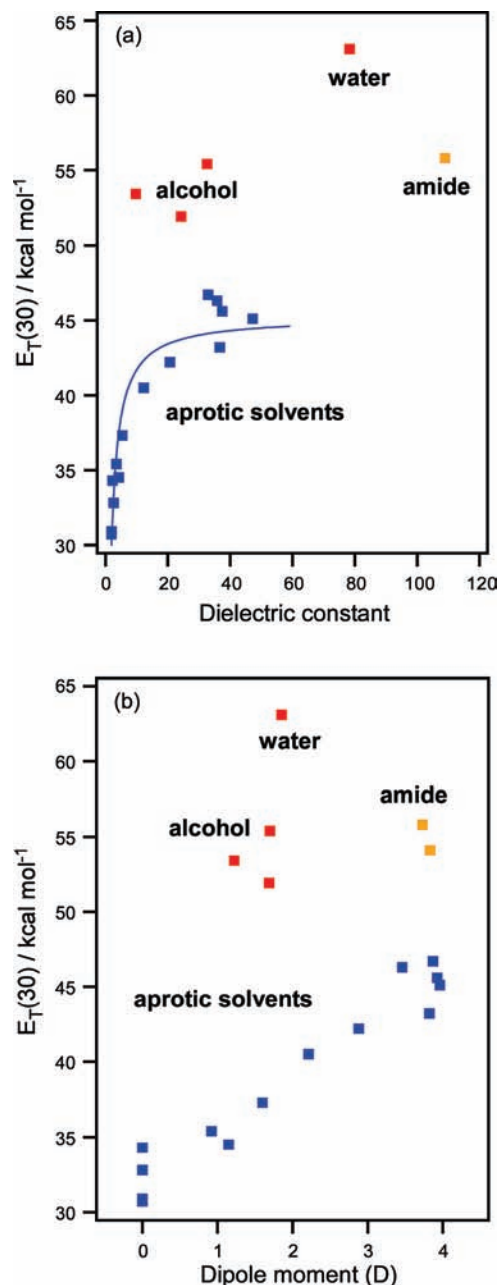


Figure 1. (a) Plot of $E_T(30)$ values against dielectric constants for several solvents. The solid curve for aprotic solvents was obtained by a least-squares fit with Onsager reaction field model.² (b) Plot of $E_T(30)$ values against molecular dipole moments for the same solvents. A list for the solvents and their constants due to refs 11 and 13 is provided in the Supporting Information.

character and solvation structure might be the first clue to find the “missing link” between the empirical intuition and theoretical understanding. The absorption band of betaine-30 is attributed to an intramolecular charge-transfer (ICT) transition, whereas the molecule is too complicated to carry out a quantitative analysis on the overall solvation effect. Aromatic ketyl anions,^{17–27} benzophenone (Bp^-) and 9-fluorenone (Fl^-) radical anions, were reported to exhibit a similar blue-shifting absorption band, which is also assigned to an ICT transition involving the excess electron. Recently, by using a technique of gas-phase photodetachment spectroscopy, we have found that a few methanol molecules solvating Bp^- makes the absorption peak to converge nearly onto the bulk limit.^{28,30}

In this paper, we choose the ketyl anions solvated with a single polar molecule as a simpler model system to examine

the solvent effect on the electronic structure of a solute molecule having an ICT absorption band. Common properties among betaine-30 dye and the ketyl anions have been verified through quantum chemical calculations. Photoelectron spectroscopy has been utilized to reveal the solvent effect on the electronic ground state of the anions. We have also observed autodetaching excited states by photodetachment excitation spectroscopy. Combining both the spectroscopic data provides us with a new insight about the feature of solute–solvent intermolecular potential functions reflecting the magnitudes of empirical solvent polarity.

2. Experimental and Computational Methods

Experimental procedures in this work are similar to those described elsewhere.^{28–30} Microsolvated anions were generated with slow electron attachment in a supersonic expansion of a mixture of sample vapor seeded in argon gas at 2 atm. Vapor pressure of aromatic carbonyl molecules in a sample container was enhanced with heating it up to 110 °C, while solvent molecules were vaporized in a separate container at a room temperature. We chose diethyl ether (DEE), acetone (ACT), and acetonitrile (ACN) as aprotic solvents and water (H_2O) and methanol (MeOH) as protic solvents. Anionic species of interest, separated with a time-of-flight mass spectrometer, were illuminated with a light pulse when they reached a photodetachment region. In the measurements of photodetachment efficiency spectra, a signal or idler output of an optical parametric oscillator (OPO; GWU-Lasertechnik, VisIR2) was used as the excitation light source, and the detached electrons were repelled by a pulsed electric field onto a microchannel plate detector. The electron signal intensity was normalized against the target anion intensity as well as the photon flux. On the other hand, photoelectron spectra were measured with a “magnetic bottle” type spectrometer placed as an extension of the mass spectrometer. The third harmonic (355 nm; photon energy = 3.493 eV) of a Nd:YAG laser (Continuum, Surelite-II) was used for the excitation. The photoelectron energy resolution was as large as 100 meV as a result of the Doppler broadening due to a high velocity of the anions, which were not decelerated prior to the photodetachment.

All of quantum chemical calculations were performed by the *Gaussian 03* program suite.³⁴ Geometry optimization and estimation of vertical detachment energy (VDE) values for the anions were computed using the B3LYP level of theory with the 6-31+(d,p) basis set. The VDE values were estimated through electronic energy differences between the neutral and anionic ground states, at the optimized geometries for the anion. Time-dependent density functional theory (TDDFT) was applied for calculations of electronic transition energies for the anions. Electrostatic potentials were calculated with the *GaussViewW* program,³⁵ which was also used for visualization of molecular models.

3. Results and Discussion

General Argument on Solvatochromic Shifts. Because many solvatochromic dyes are recognized as an empirical solvent polarity probe, we consider a general formulation for solvatochromic shifts within the first-order perturbation on a solute molecule, before the present molecular systems are examined. In this subsection, a condition of intermolecular interactions giving a large spectral shift is explored to provide qualitative understanding in analyses of experimental results. We formalize both the gas-phase microsolvation and the complete solvation in the condensed phase, in a common framework where a large ensemble of solvent molecules is

assumed to play as one supramolecule. In this situation, the solvation energy is given by a two-body intermolecular interaction energy, which was formulated by Longuet-Higgins.^{31,32} The first-order perturbation part of solvation energy for a molecule in the electronic state k can be written as

$$E_k^{\text{sol}} = \int_{\text{whole space}} \int \int V(\mathbf{r}) \rho_k(\mathbf{r}) d^3\mathbf{r} \approx \int_{\text{solute volume}} \int \int V(\mathbf{r}) \rho_k(\mathbf{r}) d^3\mathbf{r} \quad (1)$$

where $\rho_k(\mathbf{r})$ is the expectation value of charge density for the solute molecule and $V(\mathbf{r})$ includes solute–solvent electrostatic potential terms as well as a part of induction terms due to charge-induced polarization of the solvent. The volume of the solute molecule is defined by a boundary surface on which $\rho_k(\mathbf{r})$ can be neglected. We do not consider here higher-order perturbations such as the solute–solvent charge transfer and dispersion forces involving deformation of $\rho_k(\mathbf{r})$.

The solvatochromic shift of photoabsorption energy from the ground (g) to excited (e) states is given by the difference between solvation energies in the two states. As will be described in the Appendix, it can be formulated as

$$\Delta E_{\text{eg}}^{\text{sol}} = - \int \int \int_{\text{solute volume}} \mathbf{P}_{\text{eg}}(\mathbf{r}) \cdot \mathbf{F}(\mathbf{r}) d^3\mathbf{r} \quad (2)$$

where $\mathbf{F}(\mathbf{r}) \equiv -\text{grad } V(\mathbf{r})$ is the force field on charges of the solute, due to the solvent. The physical meaning of $\mathbf{P}_{\text{eg}}(\mathbf{r})$ is interpreted as a vector representing the direction and magnitude of electron transfer under the photoabsorption. A large positive energy shift occurs on a condition that the solute molecule suffers a strong force field opposite to the direction of electron displacement. The most important conclusion is that the energy shift does not depend on the overall solvation energy but on the gradient of the interaction potential function. Some correlations will be found in the energy shifts for systems having a similar relationship between the direction of electron transfer in the solute molecule and the force field owing to the solvent coordination in the initial state.

Along the context of eq 2, we will interpret results of photodetachment experiments on microsolvated anions, which have an excited state concerned with the excess electron. Now we represent the vertical photodetachment energies from the anionic ground and excited states as VDE and VDE_{ex}, respectively, and also the vertical photoabsorption energy to the excited state as VAE. Thus, $\Delta E_{\text{eg}}^{\text{sol}}$ corresponds to ΔVAE . The solvent-induced shifts of VDE and VDE_{ex} are represented by ΔVDE and $\Delta\text{VDE}_{\text{ex}}$, which approximate to the interaction energies between the solvent and the excess electron in the respective electronic states, on the assumption that electron correlation effects in the anion are neglected.³⁰ There is a simple relationship,

$$\Delta\text{VAE} = \Delta\text{VDE} - \Delta\text{VDE}_{\text{ex}} \quad (3)$$

among the spectral shifts induced by solvation. ΔVAE and ΔVDE can be determined experimentally with photoabsorption and photoelectron spectroscopic measurements, respectively. Figure 2 shows a schematic representation for the relations between the energy shifts and the solvent force field, where the electron–solvent interaction is interpolated to a function of one representative coordinate. Photoabsorption and photodetachment correspond to finite and infinite displacements of the excess electron from the solvents, respectively. Higher-energy shifts occur in both VAE and VDE when the electron distribution is

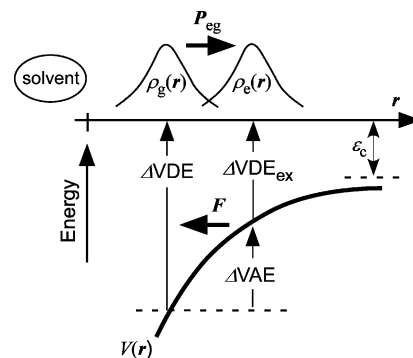


Figure 2. Schematic representation for the relationship between the transition energy shifts and electron–solvent interaction. $\rho_k(\mathbf{r})$ represents a density function for the excess electron. Actually, the signs for $\rho_k(\mathbf{r})$ and $V(\mathbf{r})$ as well as the directions for the vectors should be inverted to make an agreement with the definitions given in the Appendix, where $\rho_k(\mathbf{r})$ represents a density function for the charges rather than for electrons. The meaning of ϵ_c is presented in the Appendix.

transferred against the attractive force field due to the solvent. The empirical solvent polarity is always related to ΔVAE . As shown in eq 2, however, this value reflects only the gradient of the interaction potential energy function, $\mathbf{F}(\mathbf{r})$. ΔVDE and $\Delta\text{VDE}_{\text{ex}}$ are rather absolute indices for the potential energy depths in the electronic ground and excited states, respectively.

Electronic Properties of a Betaine-30 Molecule and Ketyl Anions with Respect to Solvent Effects. A betaine-30 molecule is too complicated to analyze its solvation further through experimental approaches. We applied quantum chemical calculations to predict the feature of solvent effects on betaine-30. Betaine-30 is totally neutral for the whole molecule, whereas the charge distribution is quite characteristic; the negative charge is accommodated almost around the phenoxide oxygen atom, and the positive charge is delocalized among the aromatic rings. Figure 3 shows contour maps of the electrostatic potential around betaine-30 in the electronic ground state, obtained with the B3LYP/6-31G(d) level calculation. Under solvation with polar solvents, solvent molecules surrounding the molecular surface of betaine-30 are probably oriented to stabilize the electrostatic energy. Thus, only a few solvent molecules within a small space adjacent to the phenoxide group are tightly bound, pointing a positive edge toward the oxygen atom. Figure 4 shows surface plots for the highest occupied molecular orbital (HOMO) and lowest unoccupied molecular orbital (LUMO) for a betaine-30 molecule. The TDDFT calculation at the same level was performed for 10 excited levels, where a strong absorption band of the first excited state (oscillator strength = 0.346) was found at $12\,183\text{ cm}^{-1}$, and other higher-energy bands are weaker by a factor of 10^{-1} . The calculated transition energy for the first excited state is slightly higher than the experimental value for that in tetramethylsilane solution ($10\,740\text{ cm}^{-1}$),¹¹ which was supposed to be close to that of the isolated molecule in the gas phase. The photoabsorption band involves a bunch of minor components other than the HOMO–LUMO transition, of which the coefficient was calculated to be as large as 0.5. The charge distributions in the excited state are hardly evaluated with the TDDFT calculation, while the transition dipole moment vector for the absorption band was found to have a very large component along the long molecular axis between the phenoxide group and the terminal phenyl group. Thus, it can be attributed to an ICT transition from the phenoxide side to the distant aromatic rings.

Because of the lack of information on the charge distributions in the excited state, we estimate the dominant effect on the

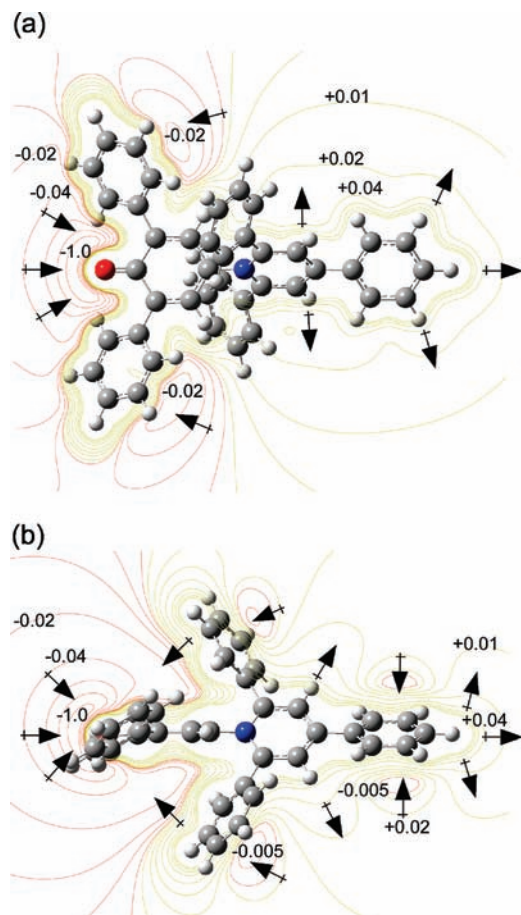


Figure 3. Contour maps of electrostatic potential around betaine-30 dye molecule obtained with the B3LYP/6-31G(d) level calculation. (a) Contours for isovalues with respect to the plane including the phenoxide group. (b) Contours for isovalues with respect to the plane perpendicular to the phenoxide group. The isovalues are shown only for representative contours. Arrows denote directions of electric field vectors but do not represent their magnitudes.

solvatochromic shifts of betaine-30 on the basis of eq 2 given in the previous subsection. Several researchers^{6–9} have already published quantitative calculations taking overall solvation effects into account. For the ICT transition, a nodal surface of the charge density change, $\Delta\rho_{eg}(\mathbf{r}) = \rho_e(\mathbf{r}) - \rho_g(\mathbf{r})$, intersects the long axis, at almost right angles (see Appendix). $\mathbf{P}_{eg}(\mathbf{r})$ takes large magnitudes around the crossing point, and orients along the long axis. A majority of solvent molecules surrounding the aromatic rings is supposed to provide weak forces almost perpendicular to the axis, because of electrostatic requirements. Thus, they are not expected to affect significantly the integral of the scalar product in eq 2. On the other hand, solvent molecules in the vicinity of the termini of the axis predominantly contribute to the force field along the axis. A strongly attractive force for electrons arises from solvent molecules tightly bound to the phenoxide side, relative to a repulsive force from those bound loosely in the opposite side. Therefore, we consider that the blue shifts of the ICT transition of betaine-30, namely the $E_T(30)$ values, originate essentially from a small number of the solvent molecules around the phenoxide oxygen atom, although the overall solvation energy is determined by interaction with a large ensemble of solvent molecules.

Aromatic ketyl anions, benzophenone and 9-fluorenone radical anions (Bp^- and Fl^-), also have a blue-shifting absorption band, which is attributed to an ICT transition of the excess electron from the carbonyl group side to the aromatic ring

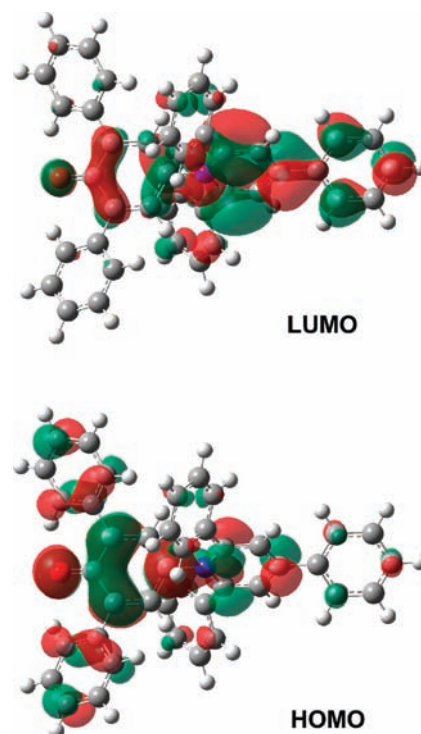


Figure 4. Surface plots of molecular orbitals involved in the blue-shifting photoabsorption band of betaine-30 dye.

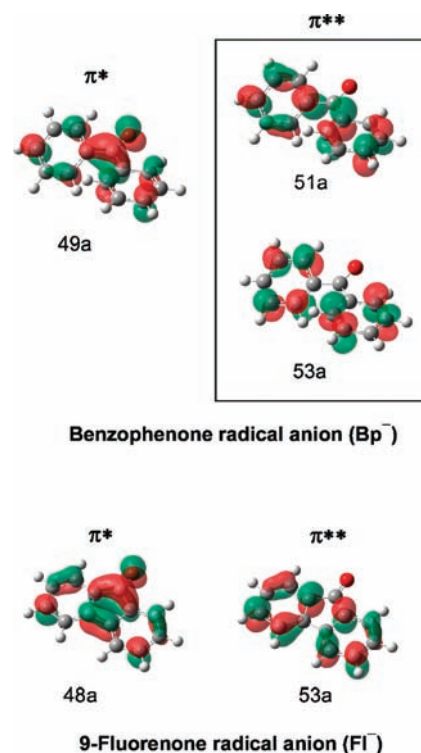


Figure 5. Surface plots of molecular orbitals involved in the blue-shifting photoabsorption band of the aromatic ketyl anions.

side.^{21,22} Approximately 30% of population for the excess electron resides in the carbonyl group both for Bp^- and Fl^- in the ground state, according to natural population analyses at the B3LYP/6-31+G(d,p) level. It is similar to the betaine-30 case that solvent molecules should tend to bind strongly to the excess negative charge on the carbonyl oxygen atom. Figure 5 shows surface plots of molecular orbitals accommodating the excess electron in the ground (π^*) and excited (π^{**}) states.

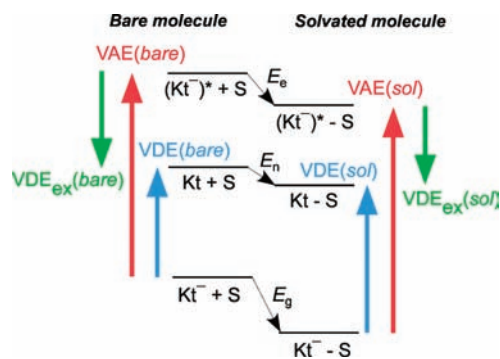


Figure 6. Schematic diagram of the energy levels for microsolvation of the ketyl anions. “Kt” and “S” represent an aromatic ketone and a solvent molecule, respectively.

The excited state of Bp^- is composed equally of two configurations, while that of Fl^- is almost a single configuration. For the bare anions in the gas phase, the energy level for the excited states lies above the electron detachment thresholds. We have already reported the photoabsorption spectrum of Bp^- by measuring the enhancement of photodetachment efficiency due to autodetachment process.²⁸ We have also revealed that the photoabsorption energy shifts for $\text{Bp}^- \cdot (\text{MeOH})_n$ are predominantly affected by the coordination number around the carbonyl group. For the solvation by MeOH, the maximal coordination number was determined to be $n = 2$, which exhibits a near convergence on the bulk limit of photoabsorption peak. The number of solvent molecules to fill the coordination space around the carbonyl group should depend on a certain volume occupied by a solvent molecule, so that the empirical solvent polarity concerning the photoabsorption energy shift should reflect the coordination number in solution phase. Actually, the $E_T(30)$ values for a same class of protic solvents tend to be large with decreasing the solvent molecular size.¹¹ In this paper, nevertheless, we focus on ketyl anions solvated with a single polar molecule, because these directly illuminate the differences in interaction potential functions discussed in the previous subsection.

Figure 6 illustrates a schematic diagram of the energy levels for microsolvation of the ketyl anions. Solvation energy for the anionic ground state (E_g) corresponds to the difference of energy minima between the bare and solvated anions. However, those for the neutral and anionic excited states (E_n and E_e) represent the energy differences under the stable nuclear geometries for the ground state, because the shifts of vertical transition energies are current interest. For the present case, vertical photodetachment energy for the excited state, VDE_{ex} , is a negative value. It is no matter for the discussion concerning the shifts of transition energies.

Photodetachment Spectroscopic Results for Microsolvated Ketyl Anions. Photoelectron (PE) and photodetachment excitation (PDE) spectra of Bp^- and Fl^- microsolvated with a single polar molecule are shown in Figure 7 and 8, respectively. In the PDE spectra, photoabsorption bands are observed as the enhancement of photodetachment efficiency due to the autodetachment process via the electronic excited states. Except for a few spectra, vibrational structures are smeared out, because of an insufficient resolution for the PE spectra, and probably because of a short lifetime of the excited state for the PDE spectra. However, apparent shifts to the higher energy side can be found in all the spectra of solvated anions. It is absolute that the shifts of vertical photodetachment energy (ΔVDE) are larger than those of photoabsorption energy (ΔVAE). This fact promises that $\Delta\text{VDE}_{\text{ex}}$ given in eq 3 is always positive.

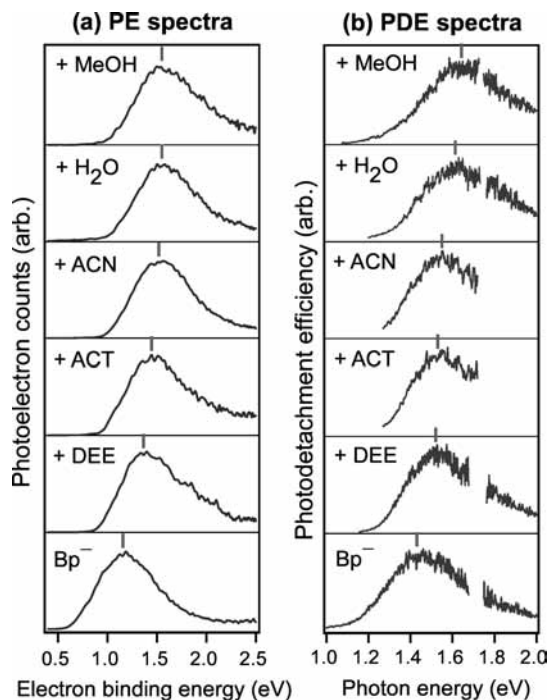


Figure 7. Photoelectron spectra (a; left) and photodetachment excitation spectra (b; right) of the benzophenone anion (Bp^-) microsolvated with a single polar molecule. Spectra of the bare anion are exhibited in the bottom. Vertical transition energies are denoted by a bar.

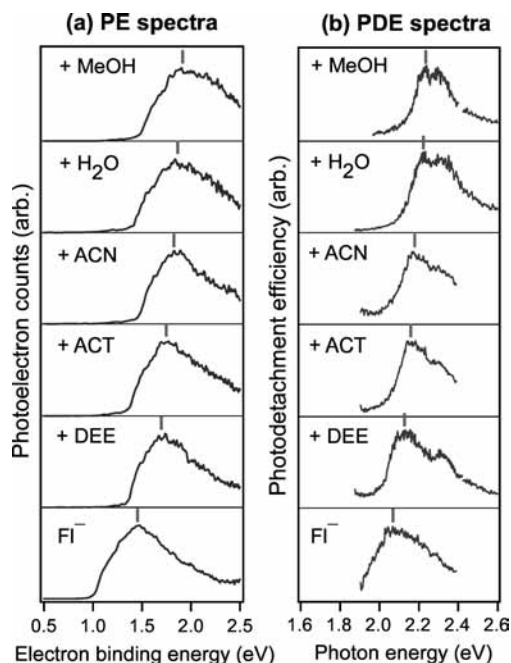


Figure 8. Photoelectron spectra (a; left) and photodetachment excitation spectra (b; right) of the 9-fluorenone anion (Fl^-) microsolvated with a single polar molecule. Spectra of the bare anion are exhibited in the bottom. Vertical transition energies are denoted by a bar.

First, we need to examine whether the present anionic systems offer a microscopic model reflecting the empirical solvent polarity. Figure 9 exhibits plots of ΔVAE values against the $E_T(30)$ scale, where a nearly linear correlation can be seen for both the solute anions. There is an exceptional trend that the largest shifts are not found for H_2O but for MeOH. At least, however, these are consistent with the fact that large magnitudes of polarity are allocated to the protic solvents. Plots of the ΔVAE values against dipole moments of the solvent molecules,

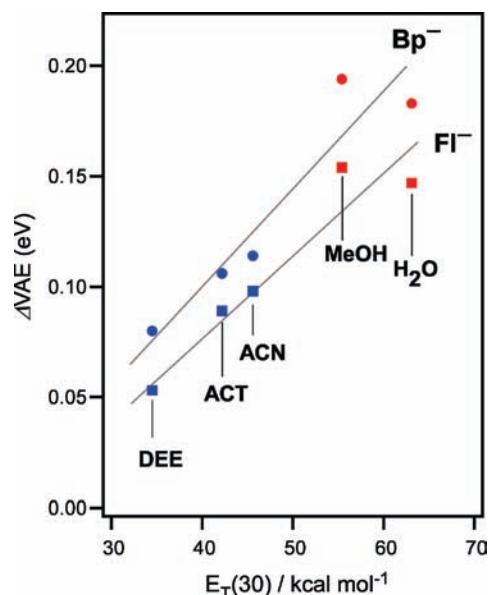


Figure 9. Plot of the observed ΔVAE values (circles for Bp^- and squares for Fl^- , respectively) against the $E_T(30)$ values of the solvents. The straight lines are appended for eye guide. The protic and aprotic solvents are represented by the red and blue markers, respectively, which are used in the other plots below.

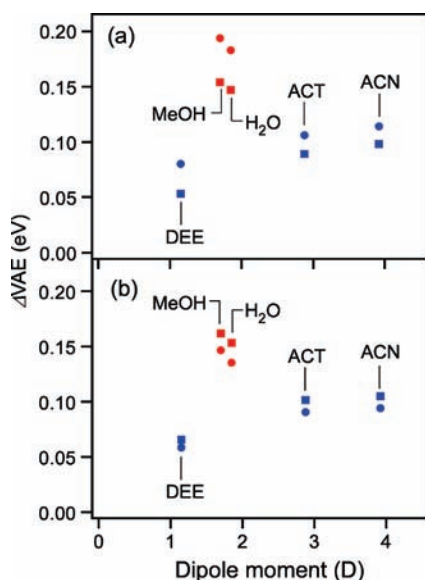


Figure 10. Plot of the ΔVAE values (circles for Bp^- and squares for Fl^- , respectively) against dipole moments of the solvent molecules. (a) Experimental values. (b) Calculated values at the B3LYP/6-31+G(d,p) level. Experimentally determined literature values¹⁵ are adopted for the dipole moments.

shown in Figure 10a, represent regular dependence for the aprotic solvents, while irregular dependence is exhibited for the protic solvents. These are the same trends as those in the $E_T(30)$ scale. Thus, we suppose that the ketyl anion systems can serve to explore the origin of the empirical polarity from a microscopic aspect.

Figure 11a shows plots of the shifts of vertical photodetachment energy for the ground and excited states (ΔVDE and ΔVDE_{ex}) with respect to the dipole moments. ΔVDE values for the aprotic solvents exhibit roughly linear correlations, suggesting that the excess electron–solvent interaction can be approximated with a charge–dipole attractive potential at a certain common distance. ΔVDE_{ex} values for these solvents are reduced in comparison with the corresponding ΔVDE values,

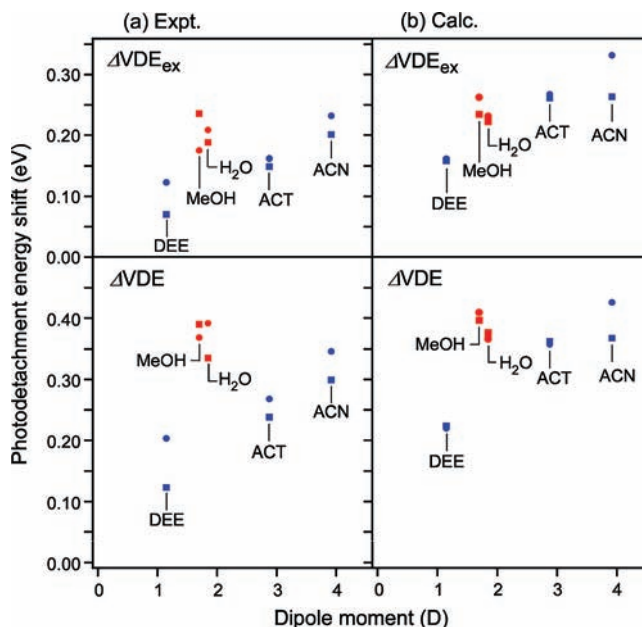


Figure 11. Plots of the shifts of vertical photodetachment energy for the ground and excited states (ΔVDE (bottom) and ΔVDE_{ex} (top)) with respect to the dipole moments. (a) Experimental values. (b) Calculated values at the B3LYP/6-31+G(d,p) level.

presumably because the average distance between the excess electron and the dipole is extended in the excited state. For the protic solvents, ΔVDE values are slightly larger than those for acetonitrile (ACN), which has the largest dipole moment in the solvents examined. On the other hand, we can find a trend that ΔVDE_{ex} values for the protic solvents are smaller than those for ACN. Adapting these results for the concept presented in Figure 2, the electron–solvent interaction energy for H_2O and $MeOH$ decreases more steeply with lengthening the electron–solvent distance, whereas the absolute interaction energy ranges are comparable with those for ACN. It indicates that the attractive interaction between the electron and the protic solvents are effective in a shorter range, in comparison with the charge–dipole interaction for the aprotic solvents.

Comparison with Theoretical Calculations. We performed quantum chemical calculations for the microsolvated ketyl anions to confirm the geometry of the solvent coordination consistent with the transition energy shifts. Figure 12 illustrates the optimized cluster structures at the B3LYP/6-31+G(d,p) level. All of the solvent molecules are attached to the oxygen end of the carbonyl group, which has considerable density of localized negative charge mainly due to the nonbonding electrons.^{28,30} The protic solvents seem to form a hydrogen bond to the nonbonding orbital in a plane defined with the carbonyl group. As seen in the previous subsection, the photoabsorption and photodetachment are involved with the excess electron in π orbitals extending to the direction perpendicular to the carbonyl plane. Therefore, the interaction between the solvents and excess electron is dominated by long-range electrostatic potential energy, where the nonbonding electrons might induce additional polarization of the solvent molecules.

The experimental and calculated transition energy values are summarized in Table 1. As shown in Figures 10b and 11b, the calculations reproduce the basic trends in the energy shifts for the protic and aprotic solvents, while the calculated ΔVDE values for the aprotic solvents are overestimated. Both in the experimental results and in theoretical calculations, the most important feature is the large photoabsorption energy shifts

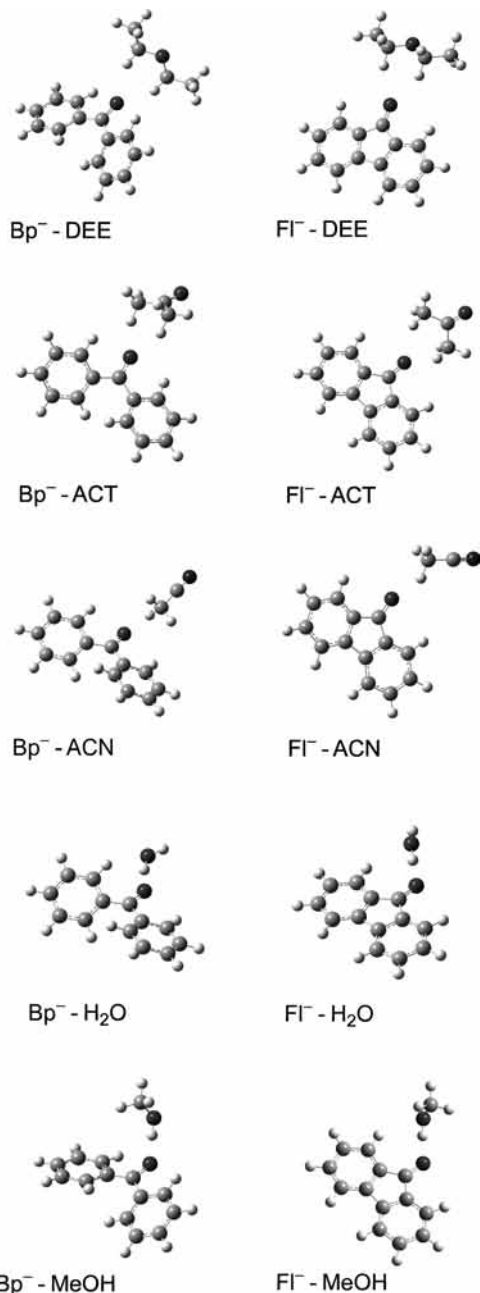


Figure 12. Optimized structures of the microsolvated ketyl anions calculated at the B3LYP/6-31+G(d,p) level.

(ΔVAE) for the protic solvents in comparison with those for ACN, which has the largest dipole moment. On the other hand, their ΔVDE range is similar to that for ACN. Thus, we hereafter focus on the difference between H₂O and ACN in the interaction with a negative charge.

Relationship between the Solvent Polarity and Intermolecular Potential Function. As discussed in the previous subsections, the solvent polarity is essentially related to the force on electrons transferring away from (or heading to) the solvent molecules. Effective strength of the attractive force originates dominantly from the electrostatic interaction between a negative charge and a solvent molecule, where the shortest electron-solvent distance is restricted by the exchange repulsion. In this sense, a similar feature of force must be reflected in the shape of the potential energy function with respect to the distance between a solvent molecule and a localized negative charge, namely, an atomic negative ion. Microsolvation of the chloride

TABLE 1: Experimental and Calculated Values of Vertical Photodetachment Energy (VDE) and Photoabsorption Energy (VAE) for the Microsolvated Ketyl Anions

anion	solvent	VDE (eV)		VAE (eV)	
		expt ^a	calcd	expt ^b	calcd
Bp^-	none	1.18	0.912	1.44	1.772
	DEE	1.39	1.131	1.52	1.831
	ACT	1.45	1.270	1.54	1.863
	ACN	1.53	1.337	1.55	1.867
	H ₂ O	1.57	1.278	1.62	1.908
	MeOH	1.55	1.321	1.63	1.919
FI^-	none	1.46	1.346	2.07	2.334
	DEE	1.58	1.570	2.13	2.400
	ACT	1.69	1.708	2.16	2.436
	ACN	1.75	1.714	2.17	2.439
	H ₂ O	1.79	1.722	2.22	2.488
	MeOH	1.85	1.742	2.23	2.496

^a Values involve an error of ± 0.04 eV. ^b Values involve an error of ± 0.02 eV.

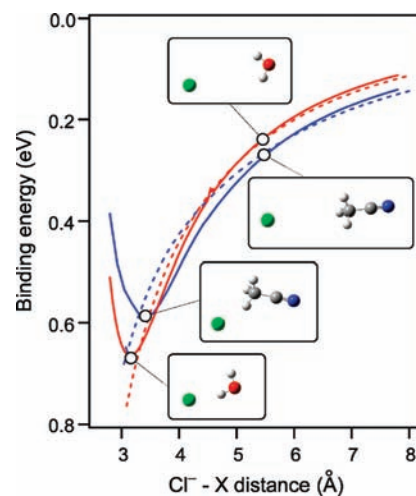


Figure 13. Intermolecular potential energy curves for Cl^- solvated with a single polar molecule (the red curve for H₂O, and the blue curve for ACN, respectively), calculated at the MP2/6-31++G(d,p) level, as a function of the distance between Cl^- and the central atom X of the solvents (X = the oxygen atom for H₂O, and X = the carbon atom in the methyl group for ACN). Broken curves represent the electrostatic energies (see text). Optimized geometries at two distances for each Cl^- -solvent pair are appended as boxed figures.

anion (Cl^-) would be a simple model system to demonstrate this idea. The microsolvated anions, $\text{Cl}^- \cdot (\text{H}_2\text{O}/\text{ACN})$, have been studied with various methods.³⁶⁻⁴² Nevertheless, only limited knowledge of the intermolecular potential energy functions has been derived experimentally. Enthalpy changes for solvation of Cl^- with a single solvent molecule were measured to be 14.7 kcal/mol (0.64 eV) for H₂O and 13.6 kcal/mol (0.59 eV) for ACN, respectively, by using high-pressure mass spectrometry.³⁷⁻³⁹ These two comparable values show that the depth of the potential has no relationship with magnitudes of the solvent polarity. Then, we performed quantum chemical calculations at the MP2/6-31++G(d,p) level for the intermolecular potential functions of $\text{Cl}^- \cdot (\text{H}_2\text{O}/\text{ACN})$. The calculated functions are shown as solid curves in Figure 13, where full optimization was done for all coordinates other than the anion-solvent distances. The calculations do not include corrections for zero-point energy and basis set superposition error. The depths of the potential curves for the two solvents are comparable, being in agreement with the experimental determinations. However,

the gradients of the potential energy functions are quite different in the attractive region. The maximal magnitudes of the force are found to be 0.119 for $\text{Cl}^- \cdot \text{H}_2\text{O}$ and 0.069 for $\text{Cl}^- \cdot \text{ACN}$, respectively, in units of $\text{eV}/\text{\AA}$. A larger energy change occurs for $\text{Cl}^- \cdot \text{H}_2\text{O}$ in the course of a finite separation from the equilibrium distance. This feature is consistent with the physical picture on the results of our photodetachment spectroscopic measurements for the microsolvated ketyl anions.

We consider the origin of the feature of the potential energy functions. Broken lines in Figure 13 represent the anion–solvent electrostatic energy functions, where point charges are distributed onto each atomic center to reproduce electric field derived from the SCF density.⁴³ In the calculation, the intermolecular bond angles were optimized, while the intramolecular geometries and charge distributions were fixed to those for the bare solvent molecules. The electrostatic energy functions exhibit fairly good correspondence with the ab initio potential energy functions in the attractive region. At a long anion–solvent distance, the potential energy is more stabilized for $\text{Cl}^- \cdot \text{ACN}$, as it is predicted with the charge–dipole interaction motif. With shortening the distance, molecular shape and charge distribution of the solvent become more effective. For ACN, the carbon atom of the CN group holds the most significant positive charge for the anion binding. The less polarized methyl group interrupts the CN group getting into contact with the anion, so that exchange repulsion occurs before the attractive interaction becomes large. On the other hand, a water molecule has proton-like hydrogen atoms on the molecular edge. One of the hydrogen atoms can approach the anion much closer, because the effective region of the repulsion is much smaller for the hydrogen atom.

There must be considerable effects other than the electrostatic interaction giving rise to both repulsive and attractive forces in a hydrogen bond. Especially, a covalent nature of a hydrogen bond is frequently debated. However, several methods of energy decomposition^{44–46} suggested that the contribution from the intermolecular charge transfer is as small as 10% of the electrostatic energy in the attractive part at the equilibrium geometries for moderate hydrogen-bonded systems. In our ab initio calculations for $\text{Cl}^- \cdot \text{H}_2\text{O}$, natural charge on the Cl atom was determined to be -0.961 at the equilibrium distance (3.15 \AA), and to be -0.991 at the distance of the maximal attractive force (3.65 \AA). It seems consistent with that the covalent interactions decrease rapidly with lengthening the intermolecular distance, and that the potential curve in the shorter attractive region for $\text{Cl}^- \cdot \text{H}_2\text{O}$ can be approximated by the electrostatic energy alone. Such an idea might also serve as a plausible reason why the Buckingham–Fowler model⁴⁷ assuming the electrostatic interaction as well as a repulsive hard-sphere often reproduces the exact geometries of hydrogen-bonded complexes. Thus, we conclude that a large “polarity” for a protic solvent dominantly reflects the effectual electrostatic force to a negative charge in the shorter attractive region.

4. Concluding Remarks

In this paper, we have discussed the microscopic background of the empirical solvent polarity with the aid of photodetachment spectroscopic experiments and theoretical calculations. It can be interpreted as a trend in the strength of the attractive forces between solvents and a negative charge. A large “polarity” for protic solvents is essentially attributed to a large gradient of the interaction potential energy function in a short-range. However, it is necessary for quantitative analyses of behavior of real solution systems to include effects ignored in this study, such as the higher-order perturbations and multibody effects.

Especially, the reason for a large polarity of bulk water relative to methanol should be verified with considering a trend in the coordination number of solvent molecules around a negatively charged site of a solute molecule. Moreover, of course, our interpretation cannot be applied for solvent effects on solute molecules having a significant positively charged site involved in ICT transitions, because the initial force field due to the solvents might be quite different. We have proposed just a fundamental point of view for a typical case of solvent polarity parameters.

Finally, we should mention how the empirical solvent polarity affects ionic reaction rates of organic compounds in the solution phase, because these often exhibit a nice correlation, as referred to in the Introduction. In many organic chemistry textbooks following the conventional Hughes–Ingold interpretation,⁴⁸ an extraordinary change of the rates of nucleophilic reactions in protic solvents is explained qualitatively with respect to the anion–solvent hydrogen bonding energy, which is assumed to be much larger than the interaction energy between the anion and aprotic solvents. However, as shown in the present study, such explanation is not adequate, because the reactions must proceed under a solvated condition without breaking the intermolecular bonds into infinite separation. In other words, the reaction processes are independent of the overall solvation energy. The reactions exhibiting correlations with the solvent polarity parameters involve an activation barrier due to forward or backward electron transfer of a finite distance with regard to a negatively charged site of the reactants. Thus, a solvent force field around the anionic site might be responsible for the energy difference from the reactant state to the transition state, leading to the change of the reaction rate. This simple scenario is proposed on the basis of our interpretation of the solvent polarity.

Acknowledgment. T.M. thanks the Japan Society of the promotion of Science for financial support by the Grant-in-Aid for Scientific Research (No. 19550003). This work is partially supported by the Grant-in-Aid for Scientific Research on Priority Areas “Molecular Science for Supra Functional Systems” (No. 477) from the Ministry of Education, Culture, Sports, Science, and Technology (MEXT) of Japan.

Appendix: Formulation of solvatochromic shifts within the first-order perturbation

The first-order perturbation part of solvation energy in the electronic state k is given by

$$E_k^{\text{sol}} \approx \iiint_{\text{solute volume}} V(\mathbf{r}) \rho_k(\mathbf{r}) d^3\mathbf{r} \quad (\text{A1})$$

If the nuclear motions are frozen, $\rho_k(\mathbf{r})$ is expressed by

$$\rho_k(\mathbf{r}) = -\iiint \psi_k^* \psi_k \sum_n \delta(\mathbf{r}_n - \mathbf{r}) \prod_n d^3\mathbf{r}_n + \sum_N \delta(\mathbf{r}_N - \mathbf{r}) Z_N \quad (\text{A2})$$

where the first and second terms correspond to the electronic and nuclear parts, respectively. ψ_k represents the electronic wave function, and Z_N is the atomic number for nuclear charges. Solvatochromic shift of photoabsorption energy from the ground (g) to excited (e) states is considered to be the difference of perturbation energies between the two states, which is given

by

$$\Delta E_{\text{eg}}^{\text{sol}} = \iiint_{\text{solute volume}} V(\mathbf{r}) \Delta \rho_{\text{eg}}(\mathbf{r}) d^3\mathbf{r} \quad (\text{A3})$$

where $\Delta \rho_{\text{eg}}(\mathbf{r}) = \rho_e(\mathbf{r}) - \rho_g(\mathbf{r})$. The nuclear part in $\Delta \rho_{\text{eg}}(\mathbf{r})$ is canceled, because the absorption peak corresponds to the vertical transition without nuclear displacements. By the same reason for the solvent remaining stationary during the photoabsorption, $V(\mathbf{r})$ keeps the initial form due to a solvent coordination in the ground state.

It is assumed that $\Delta \rho_{\text{eg}}(\mathbf{r})$ can be represented by the divergence of a vector $\mathbf{P}_{\text{eg}}(\mathbf{r})$:

$$\Delta \rho_{\text{eg}}(\mathbf{r}) \equiv -\text{div } \mathbf{P}_{\text{eg}}(\mathbf{r}) \quad (\text{A4})$$

$\mathbf{P}_{\text{eg}}(\mathbf{r})$ is interpreted as a vector representing the direction and magnitude of electron transfer under the photoabsorption, by analogy with the equation of relationship between the density $\rho(\mathbf{r},t)$ and velocity $\mathbf{j}(\mathbf{r},t)$ of a fluid,

$$\frac{d\rho(\mathbf{r},t)}{dt} = -\text{div } \mathbf{j}(\mathbf{r},t) \quad \mathbf{P}_{\text{eg}}(\mathbf{r}) = \int \mathbf{j}(\mathbf{r},t) dt$$

The explicit form of $\mathbf{P}_{\text{eg}}(\mathbf{r})$ can be formulated as

$$\mathbf{P}_{\text{eg}}(\mathbf{r}) = -\frac{1}{4\pi} \iiint \frac{\mathbf{r} - \mathbf{r}'}{|\mathbf{r} - \mathbf{r}'|^3} \Delta \rho_{\text{eg}}(\mathbf{r}') d^3\mathbf{r}' \quad (\text{A5})$$

by solving a Poisson equation. The relationship between $\Delta \rho_{\text{eg}}(\mathbf{r})$ and $\mathbf{P}_{\text{eg}}(\mathbf{r})$ is similar to that between a charge distribution function and its electrostatic field vector in classical electromagnetics. Thus, a large magnitude of $\mathbf{P}_{\text{eg}}(\mathbf{r})$ appears at a nodal surface of $\Delta \rho_{\text{eg}}(\mathbf{r})$, to which the direction of $\mathbf{P}_{\text{eg}}(\mathbf{r})$ is perpendicular. For the intramolecular electronic transition, $\mathbf{P}_{\text{eg}}(\mathbf{r}) \rightarrow \mathbf{0}$ at the molecular surface, and the number of electrons is unchanged:

$$\iiint_{\text{solute volume}} \Delta \rho_{\text{eg}}(\mathbf{r}) d^3\mathbf{r} = \oint_{\text{solute surface}} \mathbf{P}_{\text{eg}}(\mathbf{r}) \cdot \mathbf{n} dS = 0 \quad (\text{A6})$$

where \mathbf{n} is the normal vector on the surface.

Using the vector $\mathbf{P}_{\text{eg}}(\mathbf{r})$, eq A3 is transformed into the following:

$$\begin{aligned} \Delta E_{\text{eg}}^{\text{sol}} &= - \iiint_{\text{solute volume}} V(\mathbf{r}) \text{div } \mathbf{P}_{\text{eg}}(\mathbf{r}) d^3\mathbf{r} \\ &= - \iiint_{\text{solute volume}} \text{div}[V(\mathbf{r}) \mathbf{P}_{\text{eg}}(\mathbf{r})] d^3\mathbf{r} + \\ &\quad \iiint_{\text{solute volume}} \mathbf{P}_{\text{eg}}(\mathbf{r}) \cdot \text{grad } V(\mathbf{r}) d^3\mathbf{r} \end{aligned} \quad (\text{A7})$$

The first term vanishes, because of the Gauss' theorem:

$$\begin{aligned} \iiint_{\text{solute volume}} \text{div}[V(\mathbf{r}) \mathbf{P}_{\text{eg}}(\mathbf{r})] d^3\mathbf{r} \\ = \oint_{\text{solute surface}} V(\mathbf{r}) \mathbf{P}_{\text{eg}}(\mathbf{r}) \cdot \mathbf{n} dS = 0 \end{aligned}$$

Hence, we finally obtain an equation

$$\Delta E_{\text{eg}}^{\text{sol}} = - \iiint_{\text{solute volume}} \mathbf{P}_{\text{eg}}(\mathbf{r}) \cdot \mathbf{F}(\mathbf{r}) d^3\mathbf{r} \quad (\text{A8})$$

which is identical with eq 2 in the text.

Next, we consider the solvent-induced shift for photodetachment (or photoionization) energy. When electron density of the electron-detached state (n) is represented by $\rho_n(\mathbf{r})$,

$$\iiint_{\text{solute volume}} \Delta \rho_{\text{ng}}(\mathbf{r}) d^3\mathbf{r} = \oint_{\text{solute surface}} \mathbf{P}_{\text{ng}}(\mathbf{r}) \cdot \mathbf{n} dS = +1 \quad (\text{A9})$$

because the solute molecule lost one negative charge in the final state. The photodetachment energy shift is obtained through an analogous way to derivation of eq A8, while the first term in eq A7 does not vanish, because $\mathbf{P}_{\text{ng}}(\mathbf{r})$ has a finite quantity on the molecular surface. Thus, the energy shift is given by

$$\Delta E_{\text{ed,g}}^{\text{sol}} = \varepsilon_c - \iiint_{\text{solute volume}} \mathbf{P}_{\text{ng}}(\mathbf{r}) \cdot \mathbf{F}(\mathbf{r}) d^3\mathbf{r} \quad (\text{A10})$$

where ε_c is the interaction energy of the solvent with the detaching electron on the molecular surface. ε_c is supposed to be considerably large in the condensed phase, where it will be comparable with the ion solvation energy in dielectric continuum estimated by the Born theory.¹ Nevertheless, for gas-phase microsolvation, ε_c is estimated to be as small as a few tens of millielectronvolts, because it will be in the same order as electron binding energy of dipole-bound anions.³³ Thus, ε_c can be neglected when we discuss energetics of microsolvated anions in the gas phase. The shift of photodetachment energy from the electronic excited state is given by

$$\Delta E_{\text{ed,e}}^{\text{sol}} = \varepsilon_c - \iiint_{\text{solute volume}} \mathbf{P}_{\text{ne}}(\mathbf{r}) \cdot \mathbf{F}(\mathbf{r}) d^3\mathbf{r} \quad (\text{A11})$$

where we assume ε_c to be almost the same as that in eq A10 because of its physical meaning. Then, we obtain the relationship between the photodetachment and photoabsorption energies:

$$\Delta E_{\text{eg}}^{\text{sol}} = \Delta E_{\text{ed,g}}^{\text{sol}} - \Delta E_{\text{ed,e}}^{\text{sol}} \quad (\text{A12})$$

by using $\mathbf{P}_{\text{eg}}(\mathbf{r}) = \mathbf{P}_{\text{ng}}(\mathbf{r}) - \mathbf{P}_{\text{ne}}(\mathbf{r})$, which is derived from eq A5. This equation is identical with eq 3 in the text.

Supporting Information Available: Solvents and their physical constants as well as $E_T(30)$ values adopted for making Figure 1 are summarized in a table. The optimized geometries in the DFT calculations for betaine-30 dye molecule and the microsolvated ketyl anions are given in Cartesian coordinates. This material is available free of charge via the Internet at <http://pubs.acs.org>.

References and Notes

- (1) Born, M. Z. *Phys.* **1920**, *1*, 45.
- (2) Onsager, L. *J. Am. Chem. Soc.* **1936**, *58*, 1486.
- (3) Ooshika, Y. *J. Phys. Soc. Jpn.* **1954**, *9*, 594.
- (4) McRae, E. G. *J. Phys. Chem.* **1957**, *61*, 562.
- (5) Karelson, M. M.; Zerner, M. C. *J. Phys. Chem.* **1992**, *96*, 6949.
- (6) Caricato, M.; Mennucci, B.; Tomasi, J. *Mol. Phys.* **2006**, *104*, 875.
- (7) Mente, S. R.; Maroncelli, M. *J. Phys. Chem. B* **1999**, *103*, 7704.

- (8) Lobaugh, J.; Rossky, P. J. *J. Phys. Chem. A* **2000**, *104*, 899.
- (9) Ishida, T.; Rossky, P. J. *J. Phys. Chem. A* **2001**, *105*, 558.
- (10) Reichardt, C. *Angew. Chem., Int. Ed.* **1965**, *4*, 29.
- (11) Reichardt, C. *Chem. Rev.* **1994**, *94*, 2319.
- (12) Katritzky, A. R.; Fara, D. C.; Yang, H.; Tamm, K.; Tamm, T.; Karelson, M. *Chem. Rev.* **2004**, *104*, 175.
- (13) Lide, D. R., Ed. *CRC Handbook of Chemistry and Physics*, 74th ed.; CRC Press, Inc.: Boca Raton, FL, 1993.
- (14) Abraham, M. H.; Grellier, P. L.; Nasehzadeh, A.; Walker, R. A. C. *J. Chem. Soc., Perkin Trans.* **1988**, *2*, 1717.
- (15) Taft, R. W.; Kalmét, M. J. *J. Am. Chem. Soc.* **1976**, *98*, 2886.
- (16) Marcus, Y. *J. Sol. Chem.* **1991**, *20*, 929.
- (17) Hayon, E.; Ibata, T.; Lichtin, N. N.; Simic, M. *J. Phys. Chem.* **1972**, *76*, 2072.
- (18) Hoshino, M.; Arai, S.; Imamura, M. *J. Phys. Chem.* **1974**, *78*, 1473.
- (19) Marignier, J. L.; Hickel, B. *J. Phys. Chem.* **1984**, *88*, 5375.
- (20) Lin, Y.; Jonah, C. D. *J. Phys. Chem.* **1992**, *96*, 10119.
- (21) Shida, T.; Hamill, W. H. *J. Am. Chem. Soc.* **1966**, *88*, 1683.
- (22) Shida, T.; Iwata, S.; Imamura, M. *J. Phys. Chem.* **1974**, *78*, 741.
- (23) Ichikawa, T.; Ishikawa, Y.; Yoshida, H. *J. Phys. Chem.* **1988**, *92*, 508.
- (24) Shida, T. *Electronic Absorption Spectra of Radical Ions*; Elsevier: Amsterdam, 1988.
- (25) Wagner-Czauderna, E.; Lipka, R.; Kalinowski, M. K. *Ber. Bunsenges. Phys. Chem.* **1997**, *101*, 668.
- (26) Tachikawa, H.; Iyama, T. *Phys. Chem. Chem. Phys.* **2002**, *4*, 5806.
- (27) Ichikawa, T.; Ueda, K.; Yoshida, H. *Bull. Chem. Soc. Jpn.* **1991**, *64*, 2695.
- (28) Yagi, I.; Maeyama, T.; Fujii, A.; Mikami, N. *J. Phys. Chem. A* **2007**, *111*, 7646.
- (29) Maeyama, T.; Yagi, I.; Murota, Y.; Fujii, A.; Mikami, N. *J. Phys. Chem. A* **2006**, *110*, 13712.
- (30) Maeyama, T.; Yagi, I.; Fujii, A.; Mikami, N. *Chem. Phys. Lett.* **2008**, *457*, 18.
- (31) Longuet-Higgins, H. C. *Proc. R. Soc. A* **1956**, *235*, 537.
- (32) Stone, A. J. *The Theory of Intermolecular Forces*; Oxford University Press: Oxford, U.K., 1996.
- (33) Simons, J. *J. Phys. Chem. A* **2008**, *112*, 6401.
- (34) Frisch, M. J.; Trucks, G. W.; Schlegel, H. B.; Scuseria, G. E.; Robb, M. A.; Cheeseman, J. R.; Montgomery, Jr., J. A.; Vreven, T.; Kudin, K. N.; Burant, J. C.; Millam, J. M.; Iyengar, S. S.; Tomasi, J.; Barone, V.; Mennucci, B.; Cossi, M.; Scalmani, G.; Rega, N.; Petersson, G. A.; Nakatsuji, H.; Hada, M.; Ehara, M.; Toyota, K.; Fukuda, R.; Hasegawa, J.; Ishida, M.; Nakajima, T.; Honda, Y.; Kitao, O.; Nakai, H.; Klene, M.; Li, X.; Knox, J. E.; Hratchian, H. P.; Cross, J. B.; Bakken, V.; Adamo, C.; Jaramillo, J.; Gomperts, R.; Stratmann, R. E.; Yazyev, O.; Austin, A. J.; Cammi, R.; Pomelli, C.; Ochterski, J. W.; Ayala, P. Y.; Morokuma, K.; Voth, G. A.; Salvador, P.; Dannenberg, J. J.; Zakrzewski, V. G.; Dapprich, S.; Daniels, A. D.; Strain, M. C.; Farkas, O.; Malick, D. K.; Rabuck, A. D.; Raghavachari, K.; Foresman, J. B.; Ortiz, J. V.; Cui, Q.; Baboul, A. G.; Clifford, S.; Cioslowski, J.; Stefanov, B. B.; Liu, G.; Liashenko, A.; Piskorz, P.; Komaromi, I.; Martin, R. L.; Fox, D. J.; Keith, T.; Al-Laham, M. A.; Peng, C. Y.; Nanayakkara, A.; Challacombe, M.; Gill, P. M. W.; Johnson, B.; Chen, W.; Wong, M. W.; Gonzalez, C.; Pople, J. A. *Gaussian 03*; Gaussian, Inc.: Wallingford, CT, 2004.
- (35) Dennington II, R.; Keith, T.; Millam, J. *GaussViewW*, Version 4.1; Semichem, Inc.: Shawnee Mission, KS, 2007.
- (36) Xantheas, S. S. *J. Phys. Chem.* **1996**, *100*, 9703.
- (37) Arshadi, M.; Yamdagni, R.; Kebarle, P. *J. Phys. Chem.* **1970**, *74*, 1475.
- (38) Yamdagni, R.; Kebarle, P. *J. Am. Chem. Soc.* **1972**, *94*, 2940.
- (39) Hiraoka, K.; Mizuse, S.; Yamabe, S. *J. Phys. Chem.* **1988**, *92*, 3943.
- (40) Markovich, G.; Pollack, S.; Giniger, R. *Cheshnovsky J. Chem. Phys.* **1994**, *101*, 9344.
- (41) Markovich, G.; Perera, L.; Berkowitz, M. L. *Cheshnovsky J. Chem. Phys.* **1996**, *105*, 2675.
- (42) Roscioli, J. R.; Diken, E. G.; Johnson, M. A.; Horvath, S.; McCoy, A. B. *J. Phys. Chem. A* **2006**, *110*, 4943.
- (43) Singh, U. C.; Kollman, P. A. *J. Comput. Chem.* **1984**, *5*, 129.
- (44) Kitaura, K.; Morokuma, K. *Int. J. Quantum Chem.* **1976**, *10*, 325.
- (45) Glendening, E. F.; Streitwieser, A. *J. Chem. Phys.* **1994**, *100*, 2900.
- (46) Pendás, A. M.; Blanco, M. A.; Francisco, E. *J. Chem. Phys.* **2006**, *125*, 184112.
- (47) Buckingham, A. D.; Fowler, P. W. *J. Chem. Phys.* **1983**, *79*, 6426.
- (48) Hughes, E. D.; Ingold, C. K. *J. Chem. Soc.* **1935**, 244.